

# An IDM-based Distributionally Robust Economic Dispatch Model for Integrated Electricity-heat-gas Microgrid Considering Wind Power

Yang Liu, Xianbang Chen, *Student Member, IEEE*, Lei Wu, *Senior Member, IEEE*, and Yanli Ye

**Abstract**—Multi-energy microgrid, such as the integrated electricity-heat-gas microgrid (IEHS-MG), has been widely recognized as one of the most convenient ways to connect wind power (WP). However, the inherent intermittency and uncertainty of WP still render serious power curtailment in the operation. To this end, this paper presents an IEHS-MG model equipped with power-to-gas technology, thermal storage, electricity storage, and electrical boiler for improving the WP utilization efficiency. Moreover, a two-stage distributionally robust economic dispatch model is constructed for the IEHS-MG, with the objective of minimizing the total operational costs. The first stage determines the day-ahead decisions including on/off state and set-point decisions. The second stage adjusts the day-ahead decision according to real-time WP realization. Furthermore, WP uncertainty is characterized through an Imprecise Dirichlet model (IDM) based ambiguity set. Finally, Column-and-Constraints Generation method is utilized to solve the model, which provides a day-ahead economic dispatch strategy that immunizes against the worst-case WP distributions. Case studies demonstrate that the presented IEHS-MG model outperforms traditional IEHS-MG model in terms of WP utilization and dispatch economics, and that distributionally robust optimization can handle uncertainty effectively.

**Index Terms**—Wind power, Integrated electricity-heat-gas microgrid, Distributionally robust optimization, Day-ahead economic dispatch, Data-driven, Imprecise Dirichlet model.

## NOMENCLATURE

### Sets and indices

$t/\mathcal{T}$	Index/set of hour.
$i/\mathcal{I}$	Index/set of DERs.
$DA/RT$	Index of day-ahead/real-time decisions.
<i>Day-ahead variables</i>	
$P_{DA,t}^{MT}/P_{DA,t}^{FC}$	MT/FC power at hour $t$ .
$P_{DA,t}^{PtG}/P_{DA,t}^{EB}$	PtG/EB power at hour $t$ .
$P_{DA,t}^{buy}/P_{DA,t}^{sell}$	Buying/selling power at hour $t$ .
$P_{DA,t}^{wi}/P_{DA,t}^{wc}$	Injected/curtailed WP at hour $t$ .
$P_{DA,t}^{cha}/P_{DA,t}^{dis}$	Charge/discharge power of ESS at hour $t$ .
$Q_{DA,t}^{cha}/Q_{DA,t}^{dis}$	Charge/discharge power of TSS at hour $t$ .

Y. Liu, and Y. Ye are with the College of Electrical Engineering, Sichuan University, Chengdu, 610065, China. E-mail: yang.liu@scu.edu.cn; 2017223030033@stu.scu.edu.cn.

X. Chen and L. Wu are with the ECE Department, Stevens Institute of Technology, Hoboken, NJ 07030 USA E-mail: xchen130@stevens.edu; lei.wu@stevens.edu. (*corresponding author: Xianbang Chen*)

$Q_{DA,t}^{MT}/Q_{DA,t}^{EB}$	Heat power of MT/EB at hour $t$ .
$G_{DA,t}^{sup}/G_{DA,t}^{PtG}$	Gas power of gas supplier/PtG at hour $t$ .
$G_{DA,t}^{MT}$	MT gas consumption at hour $t$ .
$S_{DA,t}^i$	On/off state of DER $i$ at hour $t$ .
$P_{DA,t}^i$	Power of DER $i$ at hour $t$ .
$E_{DA,t}/H_{DA,t}$	SoC of ESS/TSS at hour $t$ .
$S_{DA,t}^{buy}/S_{DA,t}^{sell}$	State of buying/selling power at hour $t$ .
<i>Real-time variables</i>	
$P_{RT,t}^{MT,up}/P_{RT,t}^{MT,dn}$	Up/down regulation of MT at hour $t$ .
$P_{RT,t}^{FC,up}/P_{RT,t}^{FC,dn}$	Up/down regulation of FC at hour $t$ .
$P_{RT,t}^{EB,up}/P_{RT,t}^{EB,dn}$	Up/down regulation of EB at hour $t$ .
$P_{RT,t}^{PtG,up}/P_{RT,t}^{PtG,dn}$	Up/down regulation of PtG at hour $t$ .
$P_{RT,t}^{cha}/P_{RT,t}^{dis}$	Acutal charge/discharge power of ESS at hour $t$ .
$P_{RT,t}^{buy}/P_{RT,t}^{sell}$	Buying/selling power at hour $t$ .
$P_{RT,t}^{wi}/P_{RT,t}^{wc}$	Actual injected/curtailed WP at hour $t$ .
$P_{RT,t}^{i,up}/P_{RT,t}^{i,dn}$	Up/down regulation of DER $i$ at hour $t$ .
$Q_{RT,t}^{MT,up}/Q_{RT,t}^{MT,dn}$	Up/down regulation of MT at hour $t$ .
$Q_{RT,t}^{EB,up}/Q_{RT,t}^{EB,dn}$	Up/down regulation of EB $i$ at hour $t$ .
$Q_{RT,t}^{cha}/Q_{RT,t}^{dis}$	Acutal charge/discharge power of TSS at hour $t$ .
$G_{RT,t}^{sup,up}/G_{RT,t}^{sup,dn}$	Up/down regulation of gas supplier at hour $t$ .
$G_{RT,t}^{PtG,up}/G_{RT,t}^{PtG,dn}$	Up/down regulation of PtG at hour $t$ .
$G_{RT,t}^{MT,up}/G_{RT,t}^{MT,dn}$	Up/down regulation of MT gas consumption at hour $t$ .
$E_{RT,t}/H_{RT,t}$	SoC of ESS/TSS at hour $t$ .
<i>Parameters</i>	
$\hat{w}_t/\tilde{w}_t$	Predicted/actual WP at hour $t$ .
$\bar{P}_{RT,t}^{cha}/\bar{P}_{RT,t}^{dis}$	Maximal charge/discharge power of ESS.
$\bar{Q}_{RT,t}^{cha}/\bar{Q}_{RT,t}^{dis}$	Maximal charge/discharge power of TSS.
$\underline{E}/\bar{E}$	Minimal/maximal SoC of ESS.
$\underline{H}/\bar{H}$	Minimal/maximal SoC of TSS.
$\alpha_{FC}, \beta_{FC}$	Prices of FC generation.
$\lambda^{wc}/\lambda^{gas}$	Price of WP curtailment/gas supplier.
$\lambda^{ESS}/\lambda^{TSS}$	Operation cost of ESS/TSS.
$\lambda_t^{buy}/\lambda_t^{sell}$	Day-ahead price of buying/selling power at hour $t$ .

$\rho_t^{buy}/\rho_t^{sell}$	Real-time price of buying/selling power at hour $t$ .
$\rho^{i,up}/\rho^{i,dn}$	Price of up/down regulation of DER $i$ .
$\eta^{MT}/\eta^{EB}$	Energy efficiency of MT/EB.
$\eta^{PtG}/\eta^{gas}$	Energy efficiency of PtG/gas supplier.
$\underline{P}^i/\overline{P}^i$	Minimal/maximal power of DER $i$ .
$R^i$	Ramping capacity of DER $i$ .
$\eta^{E,cha}/\eta^{E,dis}$	Charge/discharge efficiency of ESS.
$\eta^{T,cha}/\eta^{T,dis}$	Charge/discharge efficiency of TSS.
$P_t^{load}/Q_t^{load}/G_t^{load}$	Load demand of electricity/heat/gas.
<i>Abbreviation</i>	
WP	Wind power
MEMG	Multi-energy microgrid
IEHG-MG	Integrated electricity-heat-gas microgrid
ED	Economic dispatch
DER	Distributed energy resource
CHP	Combined heat and power
EB	Electrical boiler
ESS	Electrical storage system
TSS	Thermal storage system
PtG	Power-to-gas
DO	Deterministic optimization
SO	Stochastic optimization
RO	Robust optimization
PDF	Probabilistic distribution function
DRO	Distributionally robust optimization
IDM	Imprecise Dirichlet model
FC	Fuel cell
MT	Microturbine
SoC	State of charge
MP	Master problem
SP	Subproblem
C&CG	Column-and-constraint generation
CDF	Cumulative distribution function

## I. INTRODUCTION

Energy crisis motivates the widely deployment of renewable energy sources, especially wind power (WP), in power systems [1]. Due to its flexibility, microgrid has been widely admitted as one of the most convenient ways to connect the small-scale WPs at the residential level [2]. Along with the development of multi-energy integration technology, microgrid has evolved into more flexible multi-energy microgrid (MEMG). Among various MEMGs, the integrated electricity-heat-gas microgrid (IEHG-MG) can effectively coordinate electricity, heat, and natural gas to supply various loads. Therefore, IEHG-MG and its corresponding economic dispatch (ED) modeling have attracted much attention from the academia [2]–[10].

The operational flexibility of IEHG-MG stems from controllability of various distributed energy resources (DERs) such as combined heat and power (CHP) and electrical boiler (EB). An IEHG-MG model equipped with CHP and EB is presented in

[2], [3]. The authors demonstrate that DERs enable the system to simultaneously and reliably satisfy electrical, heat, and gas loads of large-scale districts. Moreover, research [4] investigates the benefits of installing energy storage systems for example electrical storage system (ESS) and thermal storage system (TSS) in IEHG-MG, pointing out that the installation could lower the ED costs. Even though the IEHG-MGs in [2]–[4] show the remarkable ability to coordinate multi-energy flow, the fluctuation of WP could still lead to high-level WP curtailment and unsatisfied ED cost of IEHG-MG. As for this, one effective approach is to deploy the emerging power-to-gas (PtG) device as a linkage between power and gas systems, so that the excessive power can be transferred. As a result, research [5] explores the benefits to combine PtG and traditional IEHG-MG, in which the authors claim that about 50% surplus WP can be utilized for generation. Similarly, [6] also illustrates that the IEHG-MG with PtG technology outperforms traditional IEHG-MG in terms of WP utilization and daily operation cost. Furthermore, researches [7]–[10] also discuss the advantages of combining PtG and the energy storage systems in IEHG-MG, and conclude that this combination significantly enhances the energy utilization efficiency and dispatch economics of the system by effectively converting or storing abundant electricity. According to the above literatures, it is obvious that integrating CHP, ESS, TSS, EB, and PtG has great potential to improve the ED performance of IEHG-MGs.

In addition to deploying various facilities, another key element to realize the potential of IEHG-MG is applying proper methods to optimize the ED schedule. Previously, researchers prefer deterministic optimization (DO) because of its easy-to-implement and computationally efficient features [11]–[13]. However, due to the fact that DO optimistically assumes that the uncertainty factors follow the forecasting values perfectly, Li *et al.* [14] point out that the inevitable forecasting error could significantly affect solution quality of the deterministic ED. Therefore, two remarkable optimization methods, stochastic optimization (SO) and robust optimization (RO), are employed to solve the optimal ED problem. SO [15]–[17] generally characterizes the uncertainty via multiple scenarios from a predefined probabilistic distribution function (PDF). On the other hand, RO [18]–[20] focuses on the worst-case uncertainty contained in a pre-defined uncertainty set. Li *et al.* [21] present SO-based ED models for achieving cost-efficient operation of MEMGs. Based on their experiments, SO is able to economically handle uncertainties. He *et al.* [22]–[25] utilize a RO-based framework to optimize dispatch strategy for MEMGs while considering diverse uncertainties, in which RO shows remarkable robustness and security. Even though SO and RO have been proved to be effective, several issues still hinder them from wider applications. Regarding the SO, exact PDF for uncertainty is generally unavailable in practical application. In addition, the large number of scenarios of SO may result in extremely high computational time. On the other hand, RO is also concerned due to its over-conservativeness and insufficient utilization of data knowledge. To this end, the need for advanced optimization approaches has been identified as a major requirement for the efficient

implementation of ED with uncertainty.

Recently, researches have taken considerable interests in the distributionally robust optimization (DRO) approach [27], [28]. The objective of DRO is to optimize the worst-case expectation performance over a family of distributions defined by an ambiguity set. Compared to SO that requires the accurate and explicit distribution of the uncertainty variables, the ambiguity set of DRO is constructed using the statistical information which can be readily obtained from historical data. In addition, unlike RO that only focuses on the worst-case of uncertain parameters, DRO is capable of incorporating ambiguous distribution information to obtain less-conservative solutions. In research [29], a data-driven two-stage DRO based on Imprecise Dirichlet model (IDM) is presented to optimize the two-stage ED of transmission systems. The authors demonstrate the remarkable advantages of the DRO, and also point out the potential of the method in other areas of power systems.

Given the above insights, this paper presents an IDM-based DRO approach aiming at obtaining the optimal ED for an IEHG-MG considering uncertain WP. The main works of this paper are as followings.

- An IEHG-MG model containing ESS, TSS, EB, and PtG is presented. Compared to the IEHG-MGs in [2]–[10], the presented IEHG-MG can lead to a higher WP utilization and a lower ED cost, due to the integration of the flexible DERs.
- To optimize the ED for the IEHG-MG while considering WP uncertainty, an IDM-based DRO [29] is employed. By fully utilizing the uncertainty information contained in historical data, the IDM-based DRO leads to more convincing and less conservative results.
- Comprehensive experiments are performed to show the benefits of ESS, TSS, EB, and PtG in promoting WP utilization and reducing ED costs. Besides, the advantages of the presented DRO over DO, SO, and RO are also discussed.

The rest of this paper is organized as follows: section II presents the modeling of two-stage ED for the IEHG-MG; section IV presents the IDM-based DRO method for achieving the optimal ED of the IEHG-MG; section IV shows the experimental results; and section V concludes the paper.

## II. TWO-STAGE ED MODEL FOR IEHG-MG

This paper presents an IEHG-MG consisting of multiple controllable DERs to enable electric, heat, and gas supply. The details of the IEHG-MG are shown in Fig. 1.

To achieve the optimal ED while considering the uncertain WP, a two-stage ED model is established for the IEHG-MG. In the first stage, the day-ahead dispatch strategy is made to achieve the minimum operation cost based on the prediction of WP. However, the imprecise prediction of WP may result in power imbalance in the system. Therefore, the second-stage decision describes adjustment actions to compensate the power imbalance after the uncertain realization of WP.

### A. Objective Function

The objective function (1) is to minimize the total operation cost considering WP uncertainties. The total operation cost is

composed of the day-ahead dispatch cost  $C_{DA}$  and the real-time adjustment cost  $C_{RT}$ , in which  $C_{RT}$  corresponds to the adjustment cost under the worst-case WP realization.

$$\min_{\mathbf{x}} \left\{ C_{DA}(\mathbf{x}) + \max_{\tilde{\mathbf{w}}} \min_{\mathbf{y}} C_{RT}(\tilde{\mathbf{w}}, \mathbf{y}) \right\} \quad (1)$$

The first-stage decision  $\mathbf{x}$  is made in the day-ahead time frame before the WP realization  $\tilde{\mathbf{w}}$ . The day-ahead dispatch cost function is presented as in (2).

$$C_{DA} = \sum_{t \in \mathcal{T}} \left\{ \begin{array}{l} \alpha_{FC} P_{DA,t}^{FC} + \beta_{FC} P_{DA,t}^{FC} + \lambda_t^{buy} P_{DA,t}^{buy} \\ - \lambda_t^{sell} P_{DA,t}^{sell} + \lambda^{wc} P_{DA,t}^{wc} + \lambda^{gas} G_{DA,t}^{sup} \\ + \lambda^{ESS}(P_{DA,t}^{cha} + P_{DA,t}^{dis}) \\ + \lambda^{TSS}(Q_{DA,t}^{cha} + Q_{DA,t}^{dis}) \end{array} \right\} \quad (2)$$

In (2), the operation cost of fuel cell (FC) is approximated via a linear function [30]; microturbine (MT) consumes natural gas to generate electricity, therefore, the cost of MT is included in the cost of gas supply; the penalty cost of WP curtailment is included in the first stage to promote the WP utilization.

The second-stage decision  $\mathbf{y}$  describes adjustment actions after  $\tilde{\mathbf{w}}$  has been revealed in real time. The outer-layer max function searches for the worst-case distribution, while the inner-layer min function minimizes the adjustment cost under the worst case. The real-time cost function can be calculated as in (3).

$$C_{RT} = \sum_{t \in \mathcal{T}} \left\{ \begin{array}{l} \rho^{MT,up} P_{RT,t}^{MT,up} + \rho^{MT,dn} P_{RT,t}^{MT,dn} \\ + \rho^{FC,up} P_{RT,t}^{FC,up} + \rho^{FC,dn} P_{RT,t}^{FC,dn} \\ + \rho^{EB,up} P_{RT,t}^{EB,up} + \rho^{EB,dn} P_{RT,t}^{EB,dn} \\ + \rho^{PtG,up} P_{RT,t}^{PtG,up} + \rho^{PtG,dn} P_{RT,t}^{PtG,dn} \\ + \rho_t^{buy} P_{RT,t}^{buy} - \rho_t^{sell} P_{RT,t}^{sell} + \lambda^{wc} P_{RT,t}^{wc} \\ + \lambda^{ESS}(P_{RT,t}^{cha} + P_{RT,t}^{dis}) \\ + \lambda^{TSS}(Q_{RT,t}^{cha} + Q_{RT,t}^{dis}) \end{array} \right\} \quad (3)$$

where  $C_{RT}$  comprises the regulation cost of DERs including MT, FC, EB, and PtG, the regulation cost of power exchange with the main grid, and the penalty cost of WP curtailment.

### B. Day-ahead Constraints

#### 1) Power Balance Constraints:

$$\left\{ \begin{array}{l} P_{DA,t}^{MT} + P_{DA,t}^{FC} + P_{DA,t}^{dis} + P_{DA,t}^{wi} + P_{DA,t}^{buy} \\ = P_{DA,t}^{PtG} + P_{DA,t}^{load} + P_{DA,t}^{EB} + P_{DA,t}^{sell} + P_{DA,t}^{cha} \\ Q_{DA,t}^{MT} + Q_{DA,t}^{dis} + Q_{DA,t}^{EB} = Q_t^{load} + Q_t^{cha} \\ G_{DA,t}^{sup} + G_{DA,t}^{PtG} = G_t^{load} + G_{DA,t}^{MT} \end{array} \right. \quad (4)$$

Equations (4) ensure the electric, heat, and gas power balances;  $Q_{DA,t}^{MT}$  is generated by a back-pressure CHP unit which can be calculated via (5).

$$Q_{DA,t}^{MT} = \eta^{MT} P_{DA,t}^{MT} \quad (5)$$

Similarly,  $G_{DA,t}^{MT}$ ,  $G_{DA,t}^{PtG}$ , and  $Q_{DA,t}^{EB}$  are calculated as in (6).

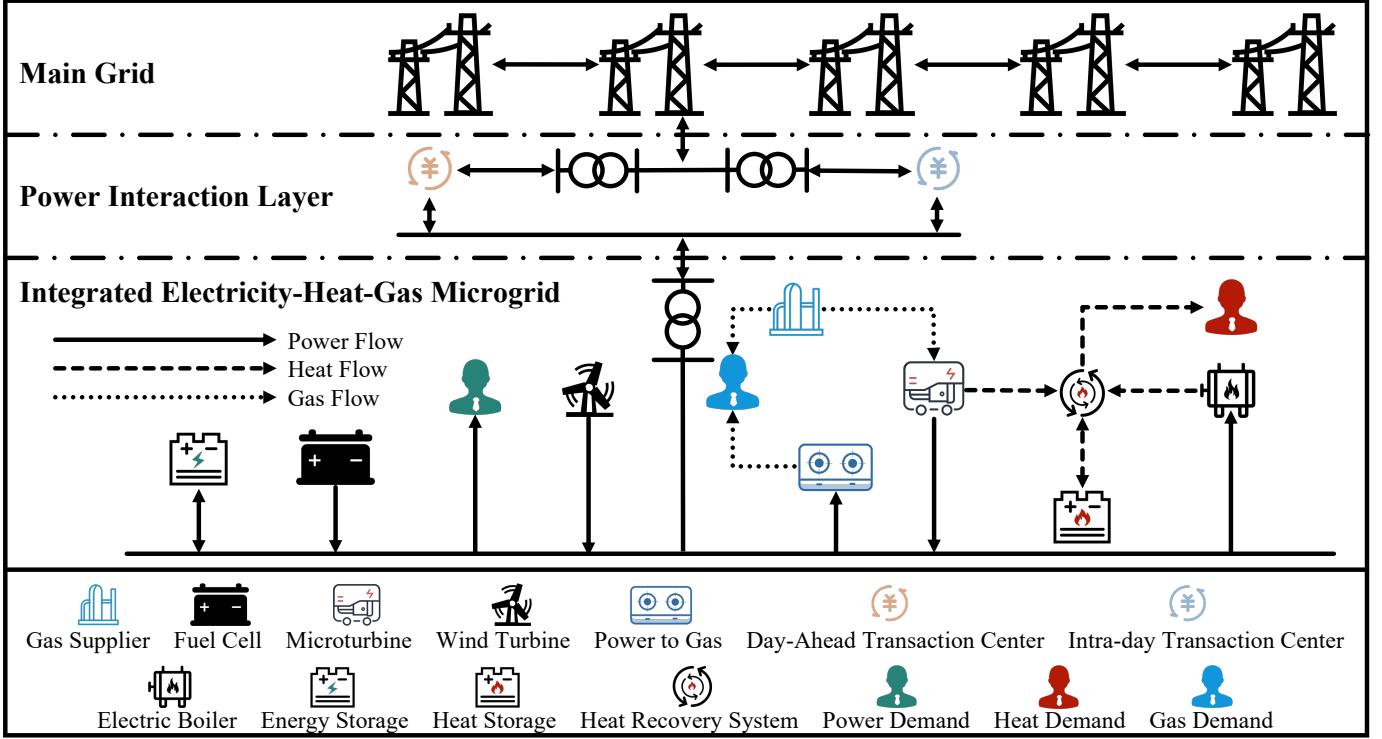


Fig. 1. Structure of the IEHG-MG model.

$$\begin{cases} G_{DA,t}^{MT} = P_{DA,t}^{MT}/\eta^{MT}, G_{DA,t}^{PtG} = \eta^{PtG} P_{DA,t}^{PtG} \\ Q_{DA,t}^{EB} = \eta^{EB} P_{DA,t}^{EB} \end{cases} \quad (6)$$

2) *Controllable DER Constraints:* For the sake of discussion, index  $i$  is used to represent certain type of DERs in the set  $\mathcal{I}$ , including MT, FC, EB, and PtG. The ramping rate and the minimum/maximum power are limited by (7)–(8).

$$\underline{P}_t^i S_{DA,t}^i \leq P_{DA,t}^i \leq \bar{P}_t^i S_{DA,t}^i \quad (7)$$

$$-R^i \leq P_{DA,t}^i - P_{DA,t-1}^i \leq R^i \quad (8)$$

3) *Energy Storage System Constraints:* Energy storage systems include ESS and TSS.

$$\begin{cases} E_{DA,t} = E_{DA,t-1} + (\eta^{E,cha} P_{DA,t}^{cha} - \frac{P_{DA,t}^{dis}}{\eta^{E,dis}}) \Delta t \\ H_{DA,t} = H_{DA,t-1} + (\eta^{T,cha} Q_{DA,t}^{cha} - \frac{Q_{DA,t}^{dis}}{\eta^{T,dis}}) \Delta t \end{cases} \quad (9)$$

$$\begin{cases} 0 \leq P_{DA,t}^{cha} \leq \bar{P}^{cha}, 0 \leq P_{DA,t}^{dis} \leq \bar{P}^{dis} \\ 0 \leq Q_{DA,t}^{cha} \leq \bar{Q}^{cha}, 0 \leq Q_{DA,t}^{dis} \leq \bar{Q}^{dis} \end{cases} \quad (10)$$

$$\begin{cases} \underline{E} \leq E_{DA,t} \leq \bar{E}, \underline{H} \leq H_{DA,t} \leq \bar{H} \\ E_{DA,1} = E_{DA,24}, H_{DA,1} = H_{DA,24} \end{cases} \quad (11)$$

Constraint (9) represents the evaluation of the stored energy considering charging and discharging efficiencies, in which  $\Delta t$  indicates 1-hour duration. Equation (10) is employed to limit the lower and upper bounds of charging and discharging

power, respectively. It is suggested that the terminal state of charge (SoC) shall be equal to the initial SoC, which is modeled as in (11).

It should be pointed out that, even though the models of energy storage system do not employ binary variables to indicate the charging/discharging state, the existence of operation costs  $\lambda^{ESS}$  and  $\lambda^{TSS}$  can avoid the situation that charging and discharging states are active simultaneously [31], [32].

4) *Power Transaction Constraints:* IEHG-MG purchases electricity from or sells electricity to the main grid for maximizing its benefits. Regarding this, the power exchange shall be limited by the transmission capacity  $P^T$  as in (12).

$$\begin{cases} 0 \leq P_{DA,t}^{sell} \leq \bar{P}^T S_{DA,t}^{sell} \\ 0 \leq P_{DA,t}^{buy} \leq \bar{P}^T S_{DA,t}^{buy} \\ S_{DA,t}^{sell} + S_{DA,t}^{buy} \leq 1 \end{cases} \quad (12)$$

5) *Wind Power Constraint:* The expected WP generation is decided based on its forecast value.

$$\begin{cases} P_{DA,t}^{wi} + P_{DA,t}^{wc} = \hat{w}_t \\ P_{DA,t}^{wi} \geq 0 \\ P_{DA,t}^{wc} \geq 0 \end{cases} \quad (13)$$

Equation (13) indicates that the expected WP curtailment shall be in the forecasted range.

### C. Real-time Constraints

1) *Power Balance Constraints:* In the real-time stage, the power balance shall be guaranteed after the uncertain WP realization is revealed, which is indicated in equation (14).

$$\left\{ \begin{array}{l} P_{DA,t}^{MT} + P_{RT,t}^{MT,up} - P_{RT,t}^{MT,dn} + P_{DA,t}^{FC} + P_{RT,t}^{FC,up} \\ \quad - P_{RT,t}^{FC,dn} + P_{RT,t}^{dis} + P_{RT,t}^{wi} + P_{DA,t}^{buy} + P_{RT,t}^{buy} \\ \quad = P_{DA,t}^{PtG} + P_{RT,t}^{PtG,up} - P_{RT,t}^{PtG,dn} + P_t^{load} + P_{DA,t}^{EB} \\ \quad + P_{RT,t}^{EB,up} - P_{RT,t}^{EB,dn} + P_{RT,t}^{cha} + P_{DA,t}^{sell} + P_{RT,t}^{sell} \\ Q_{DA,t}^{MT} + Q_{RT,t}^{MT,up} - Q_{RT,t}^{MT,dn} + Q_{RT,t}^{dis} + Q_{DA,t}^{EB} \\ \quad + Q_{RT,t}^{EB,up} - Q_{RT,t}^{EB,dn} = Q_t^{load} + Q_{RT,t}^{cha} \\ G_{DA,t}^{sup} + G_{RT,t}^{sup,up} - G_{RT,t}^{sup,dn} + G_{DA,t}^{PtG} + G_{RT,t}^{PtG,up} \\ \quad - G_{RT,t}^{PtG,dn} = G_t^{load} + G_{DA,t}^{MT} + G_{RT,t}^{MT,up} - G_{RT,t}^{MT,dn} \end{array} \right. \quad (14)$$

2) *Upward and Downward Regulation Constraints:* The power of DERs can be adjusted according to the WP realization in the real-time stage.

$$\underline{P}^i S_{DA,t}^i \leq P_{DA,t}^i + P_{RT,t}^{i,up} - P_{RT,t}^{i,dn} \leq \bar{P}^i S_{DA,t}^i \quad (15)$$

$$-R^i \leq P_{DA,t}^i + P_{RT,t}^{i,up} - P_{RT,t}^{i,dn} \quad (16)$$

$$-(P_{DA,t-1}^i + P_{DA,t-1}^{i,up} - P_{DA,t-1}^{i,dn}) \leq R^i$$

$$0 \leq P_{RT,t}^{i,up} \leq R^i, 0 \leq P_{RT,t}^{i,dn} \leq R^i \quad (17)$$

Equations (15) and (16) ensure the adjusted power and the ramping rate are within the permissible range. Equation (17) indicates the limitations on the up-regulation and down-regulation.

Up-regulation and down-regulation of gas injection of natural gas suppliers are described as in (18).

$$0 \leq G_{RT,t}^{sup,up} \leq \bar{G}^{sup}, 0 \leq G_{RT,t}^{sup,dn} \leq \bar{G}^{sup} \quad (18)$$

3) *Energy Storage System Re-dispatch Constraints:* Given the charging and discharging states, the energy storage systems can be re-dispatched according to real-time WP realization. These operational constraints are similar to the day-ahead version, which are represented as in (19)–(21).

$$\left\{ \begin{array}{l} E_{RT,t} = E_{RT,t-1} + (\eta^{E,cha} P_{RT,t}^{cha} - \frac{P_{RT,t}^{dis}}{\eta^{E,dis}}) \Delta t \\ H_{RT,t} = H_{RT,t-1} + (\eta^{T,cha} Q_{RT,t}^{cha} - \frac{Q_{RT,t}^{dis}}{\eta^{T,dis}}) \Delta t \end{array} \right. \quad (19)$$

$$\left\{ \begin{array}{l} 0 \leq P_{RT,t}^{cha} \leq \bar{P}^{cha}, 0 \leq P_{RT,t}^{dis} \leq \bar{P}^{dis} \\ 0 \leq Q_{RT,t}^{cha} \leq \bar{Q}^{cha}, 0 \leq Q_{RT,t}^{dis} \leq \bar{Q}^{dis} \end{array} \right. \quad (20)$$

$$\left\{ \begin{array}{l} \underline{E} \leq E_{RT,t} \leq \bar{E}, \underline{H} \leq H_{RT,t} \leq \bar{H} \\ E_{RT,1} = E_{RT,24}, H_{RT,1} = H_{RT,24} \end{array} \right. \quad (21)$$

4) *Power Transaction Constraints:* IEHG-MG is able to increase/reduce power exchange with the main grid for achieving power balance in the real-time stage.

$$\left\{ \begin{array}{l} 0 \leq P_{DA,t}^{sell} + P_{RT,t}^{sell} \leq \bar{P}^T S_{DA,t}^{sell} \\ 0 \leq P_{DA,t}^{buy} + P_{RT,t}^{buy} \leq \bar{P}^T S_{DA,t}^{buy} \end{array} \right. \quad (22)$$

Equation (22) guarantees that the power exchange is within the allowable range after the adjustment.

5) *Wind Power Constraint:* After obtaining the actual realization of available WP  $\tilde{w}_t$  in the real-time stage, the corresponding curtailed WP  $P_{RT,t}^{wc}$  and injected WP  $P_{RT,t}^{wi}$  can be decided. If the actual available WP is higher than the day-ahead estimation, certain WP may be curtailed. Otherwise,  $P_{RT,t}^{wc}$  may be 0, and the DERs have to increase their outputs for ensuring supply-demand balance. Although the actual available WP could be surplus or shortage, (23) ensures that the sum of  $P_{RT,t}^{wc}$  and  $P_{RT,t}^{wi}$  is equal to the actual available WP  $\tilde{w}_t$  in each hour  $t$ .

$$\left\{ \begin{array}{l} P_{RT,t}^{wi} + P_{RT,t}^{wc} = \tilde{w}_t \\ P_{RT,t}^{wi} \geq 0 \\ P_{RT,t}^{wc} \geq 0 \end{array} \right. \quad (23)$$

### III. IDM-BASED DRO MODELING AND SOLUTION

A typical DRO approach is mainly consisted of ambiguity set modeling and uncertain set transformation. Therefore, this section firstly presents the IDM which helps to establish the data-driven ambiguity set. And then the uncertain set transformation is introduced. Afterwards, WP uncertainty modeling is presented in detail. At last the implementation of DRO solution is stated.

#### A. IDM-based DRO

1) *IDM Method:* Imprecise probability theory is effective in estimating the probability of the outcomes, especially when the sample information is insufficient. Particularly, it is able to estimate the probability when prior information is scarce or even totally unknown.

In IDM, assuming that the random event  $z$  has  $n$  possible states  $(z_1, \dots, z_j, \dots, z_n)$ , the probability of each state can be presented as  $\mathcal{P}(z_j) = \theta_j$ . As a result, the set of prior Dirichlet density functions can be described as in (24).

$$\left\{ \begin{array}{l} f(\boldsymbol{\theta}) = \mathcal{G}(s) \frac{\prod_{j=1}^n \theta_j^{s \cdot r_j - 1}}{\prod_{j=1}^n \mathcal{G}(s \cdot r_j)} \\ \boldsymbol{\theta} = (\theta_1, \dots, \theta_j, \dots, \theta_n), \forall \theta_j \geq 0, \sum_{j=1}^n \theta_j = 1 \\ \forall r_j \in [0, 1], \sum_{j=1}^n r_j = 1, s = 1, j = 1, \dots, n \end{array} \right. \quad (24)$$

where  $\mathcal{G}(\cdot)$  is the Gamma function;  $\boldsymbol{\theta}$  is the vector of  $\theta_j$ ;  $r_j$  is the pre-specified weight factor;  $s$  is the sample size.

According to Bayesian rules, the corresponding posterior Dirichlet density function set can be calculated via (25), with the given number of total observations  $M_{ob}$ .

$$\left\{ \begin{array}{l} f(\boldsymbol{\theta}|M_{ob}) = \mathcal{G}(s + M_{ob}) \frac{\prod_{j=1}^n \theta_j^{m_j + s \cdot r_j - 1}}{\prod_{j=1}^n \mathcal{G}(s \cdot r_j + m_j)} \\ \sum_{j=1}^n m_j = M_{ob} \end{array} \right. \quad (25)$$

where  $m_j$  counts the times that the corresponding outcome  $z_j$  is observed.

The expected value of the posterior distribution of a random event  $z_j$  with the given  $r_j$  can be calculated as in (26).

$$E(\theta_j) = (m_j + s \cdot r_j)(s + M_{ob})^{-1} \quad (26)$$

With this, the probability intervals of the random events can be estimated from the posterior density function set as in (27).

$$\theta_j \in [\underline{E}(\theta_j), \bar{E}(\theta_j)] = \left[ \frac{m_j}{s + M_{ob}}, \frac{m_j + s}{s + M_{ob}} \right] \quad (27)$$

where  $\underline{E}(\theta_j)$  and  $\bar{E}(\theta_j)$  are the minimum and maximum expected values of the posterior probability, which are respectively evaluated with  $r_j = 0$  and  $r_j = 1$ .

Moreover, the confidence interval of  $\theta_j$  can be presented as  $[\underline{\theta}_j, \bar{\theta}_j]$ . This interval guarantees that the posterior lower probability of  $[\underline{\theta}_j, \bar{\theta}_j]$  is at the least confidence level  $\gamma$ , and the posterior upper probability of  $[\underline{\theta}_j, \bar{\theta}_j]$  is at the most  $\sigma = (1 - \gamma)/2$ , as shown in (28).

$$[\underline{\theta}_j, \bar{\theta}_j] = \begin{cases} \left[ 0, \mathcal{B}_2^{-1} \left( \frac{1+\gamma}{2} \right) \right], & m_j = 0 \\ \left[ \mathcal{B}_1^{-1} \left( \frac{1-\gamma}{2} \right), \mathcal{B}_2^{-1} \left( \frac{1+\gamma}{2} \right) \right], & 0 \leq m_j \leq n \\ \left[ \mathcal{B}_1^{-1} \left( \frac{1-\gamma}{2} \right), 1 \right], & m_j = n \end{cases} \quad (28)$$

where  $\mathcal{B}_1(\cdot)$  represents CDF of beta distribution  $\text{Beta}(m_j, s + n - m_j)$  and  $\mathcal{B}_2(\cdot)$  represents CDF of beta distribution  $\text{Beta}(s + m_j, n - m_j)$ . Based on (28), the confidence interval of CDF can be achieved. Moreover, the confidence bands of CDF become narrow as long as  $n$  grows to  $\infty$ , leading to more accurate upper and lower bounds of the confidence interval.

2) *Ambiguity Set Construction and Transformation:* It is worth noting that, the confidence bands of CDF may not contain the actual estimated interval of the random events  $[\underline{z}, \bar{z}]$ . According to research [29], this interval can be estimated via (29).

$$[\underline{z}, \bar{z}] = [z_1 - \sigma/2, z_n + \sigma/2], \sigma = (1 - \gamma)/2 \quad (29)$$

Based on the confidence interval and the associated estimation method, the ambiguity set can be obtained as (30).

$$U = \left\{ P \in U_0 ([\underline{z}, \bar{z}]) \mid \begin{array}{l} P[X \leq z_j] \in [\underline{\theta}_j, \bar{\theta}_j] \\ j = 1, \dots, n \end{array} \right\} \quad (30)$$

where  $U_0 ([\underline{z}, \bar{z}])$  represents the collection of the probability distributions, of which the actual supports are in the interval  $[\underline{z}, \bar{z}]$ . It is suggested that more sample data would lead to smaller ambiguity sets and less-conservative results.

With this, the uncertainty interval set can be estimated based on the probability points  $[\frac{1-\gamma}{2}, \frac{1+\gamma}{2}]$  on the confidence bands of cumulative distribution function (CDF).

3) *Wind Power Uncertainty Description Using Uncertainty Set:* Based on the aforementioned theoretical derivation [29], the uncertainty set of WP can be constructed via following 3 steps.

Step 1: Randomly generate  $n$  data samples and count observation times  $m_j$  for each value of WP;

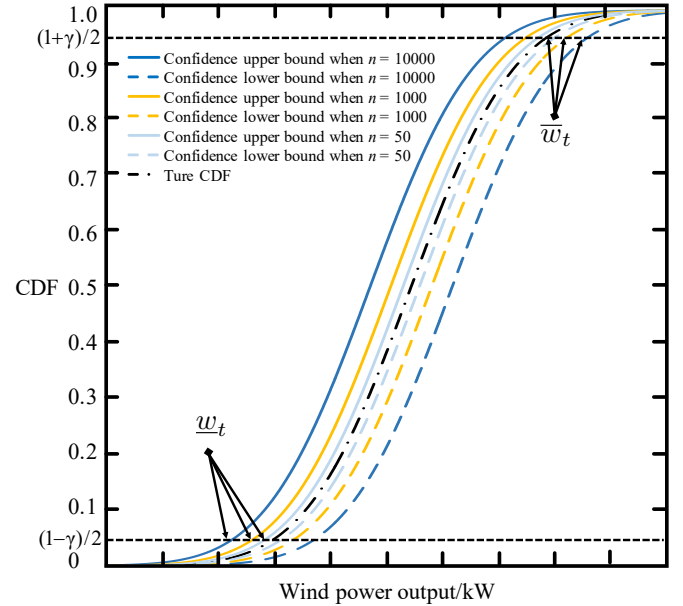


Fig. 2. Reformation process of ambiguity set to uncertainty set.

Step 2: Apply (28) to obtain the confidence bands for CDF. The confidence bands shrink as more sample data are generated, as illustrated in Fig. 2;

Step 3: Based on equation (29), estimate the probability points  $[(1 - \gamma)/2, (1 + \gamma)/2]$  on the confidence bands of CDF, as shown in Fig. 2. As a result, the corresponding interval of WP  $[\underline{w}_t, \bar{w}_t]$  on x-axis can be achieved, which is the uncertainty set of WP.

Additionally, the budget of uncertainty  $\Gamma$  is also introduced, as shown in (31).

$$\begin{cases} \tilde{w}_t = (\underline{w}_t - \hat{w}_t)\mu_t^- + (\bar{w}_t - \hat{w}_t)\mu_t^+ + \hat{w}_t \\ \sum_{t \in \mathcal{T}} (\mu_t^- + \mu_t^+) \leq \Gamma, \mu_t^- + \mu_t^+ \leq 1 \end{cases} \quad (31)$$

where  $\mu_t^+$  and  $\mu_t^-$  are 0-1 auxiliary variables.

### B. Solution Method

1) *Compact Form:* For the sake of clear presentation, the two-stage ED model is rewritten in the compact form as in (32).

$$\begin{aligned} & \min_{\mathbf{x}} \{ \mathbf{c}^\top \mathbf{x} + \max_{\tilde{\mathbf{w}}} \min_{\mathbf{y}} [\mathbf{a}^\top \mathbf{y} + \mathbf{b}^\top \tilde{\mathbf{w}}] \} \\ & \text{s.t. } \mathbf{A}\mathbf{x} \leq \mathbf{d}, \mathbf{I}\mathbf{y} \leq \tilde{\mathbf{w}}, \mathbf{B}\mathbf{x} + \mathbf{D}\mathbf{y} \leq \mathbf{f}. \end{aligned} \quad (32)$$

where  $\mathbf{a}, \mathbf{b}, \mathbf{c}, \mathbf{d}, \mathbf{f}, \mathbf{A}, \mathbf{B}, \mathbf{D}$ , and  $\mathbf{I}$  are the constant matrices and vectors.

2) *Model Decomposition:* The aforementioned two-stage ED model has a nested min-max-min structure, which is difficult to solve. Column-and-constraint generation (C&CG) algorithm is an effective method that can divide the original problem into a master problem (MP) and a subproblem (SP), which significantly facilitates the model solution. Therefore, the objective of the MP is to find the optimal  $\mathbf{x}$  with the realizations from SP1. SP1 calculates the worst case with

respect to the  $\mathbf{x}$  from MP. Optimal solution to the original solution can be achieved when the iterative process converges.

$$\text{MP: } \begin{cases} \min_{\mathbf{x}} (\mathbf{c}^\top \mathbf{x} + \varphi) \\ \text{s.t. } \varphi \geq \mathbf{a}^\top \mathbf{y} + \mathbf{b}^\top \tilde{\mathbf{w}}, \mathbf{A}\mathbf{x} \leq \mathbf{d}, \\ \quad \mathbf{I}\mathbf{y} \leq \tilde{\mathbf{w}}, \mathbf{B}\mathbf{x} + \mathbf{D}\mathbf{y} \leq \mathbf{f}. \end{cases} \quad (33)$$

$$\text{SP1: } \begin{cases} \max_{\tilde{\mathbf{w}}} \min_{\mathbf{y}} (\mathbf{a}^\top \mathbf{y} + \mathbf{b}^\top \tilde{\mathbf{w}}) \\ \text{s.t. } \mathbf{B}\mathbf{x} + \mathbf{D}\mathbf{y} \leq \mathbf{f}, \mathbf{I}\mathbf{y} \leq \tilde{\mathbf{w}}. \end{cases} \quad (34)$$

3) *The Equivalent Inner-level Problem of SP1:* SP1 employs the strong duality theory to transform the max-min structure into an equivalent single-stage problem SP2 shown in (35).

$$\text{SP2: } \begin{cases} \max_{\tilde{\mathbf{w}}, \nu, \mathbf{v}} (\mathbf{f}^\top \nu - \mathbf{x}^\top \mathbf{B}^\top \nu + \tilde{\mathbf{w}}^\top \mathbf{h}) \\ \text{s.t. } \mathbf{D}^\top \nu + \mathbf{I}^\top \mathbf{v} = \alpha, \nu, \mathbf{v} \leq 0. \end{cases} \quad (35)$$

where  $\nu$  and  $\mathbf{v}$  are the dual variables;  $\mathbf{h}$  represents the auxiliary variables. However, applying the strong duality theory introduces a bilinear term  $\tilde{\mathbf{w}}^\top \mathbf{h}$  in the objective function, making SP2 still nonlinear and difficult to solve. Therefore, the Big-M linearization method is adopted to deal with the bilinear terms in SP2. Meanwhile, the budget of uncertainty is also taken into account to constrain the uncertainty set. The converted SP2 is presented as SP3 shown in (36).

$$\text{SP3: } \begin{cases} \max_{\tilde{\mathbf{w}}, \nu, \mathbf{v}} \left\{ \mathbf{f}^\top \nu - \mathbf{x}^\top \mathbf{B}^\top \nu + \bar{\mathbf{w}}\mathbf{h}^+ + \underline{\mathbf{w}}\mathbf{h}^- \right\} \\ \text{s.t. } \mathbf{D}^\top \nu + \mathbf{I}^\top \mathbf{v} = \alpha, \nu \leq 0, \mathbf{b} + \mathbf{v} = \mathbf{h}, \mathbf{v} \leq 0, \\ \quad -M(1 - \mu_t^+) + h_t \leq h_t^+ \leq M(1 - \mu_t^+) + h_t, \\ \quad -M(1 - \mu_t^-) + h_t \leq h_t^- \leq M(1 - \mu_t^-) + h_t, \\ \quad -M\mu_t^+ \leq h_t^+ \leq M\mu_t^+, -M\mu_t^- \leq h_t^- \leq M\mu_t^-, \\ \quad \mu_t^+ + \mu_t^- \leq 1, \sum_{t \in \mathcal{T}} (\mu_t^+ + \mu_t^-) \leq \Gamma. \end{cases} \quad (36)$$

where  $M$  is a large constant;  $\mathbf{h}^+$  and  $\mathbf{h}^-$  are the positive and negative values of  $\mathbf{h}$ ;  $h_t^+$  and  $h_t^-$  represent the  $t^{th}$  component of  $\mathbf{h}^+$  and  $\mathbf{h}^-$ ;  $\bar{\mathbf{w}}$ ,  $\underline{\mathbf{w}}$ , and  $\hat{\mathbf{w}}$  represent the upper limit, lower limit, and prediction of the uncertain  $\tilde{\mathbf{w}}$ .

4) *Iterations Between MP and SP3:* A standard two-stage model is finally reformulated as MP and SP3. C&CG algorithm is used to solve the model via the following steps.

Step 1 (Initialization): Set the initial upper and lower bounds of the problem as  $UB_1 = +\infty$  and  $LB_1 = -\infty$ . Specify the maximum number of the iterations  $K$ . Set the number of iterations  $k = 1$  and the convergence gap  $\sigma > 0$ . Using WP prediction as the initial scenario.

Step 2 (MP Computation): Solve MP to get the optimal solution  $(\mathbf{x}_k^*, \varphi_k^*)$ . Update  $LB_k = \mathbf{c}^\top \mathbf{x}_k^* + \varphi_k^*$ .

Step 3 (SP3 Computation): Solve SP3 with  $\mathbf{x}_k^*$  to obtain  $(\hat{\mathbf{w}}_k^*, \mathbf{y}_k^*)$ . Update the worst-case WP scenario as  $\hat{\mathbf{w}}_{k+1} = \hat{\mathbf{w}}_k^*$  and  $UB_{k+1} = \mathbf{c}^\top \mathbf{x}_k^* + \mathbf{a}^\top \mathbf{y}_k^* + \mathbf{b}^\top \hat{\mathbf{w}}_k^*$ .

Step 4 (Check convergence): If  $UB_k - LB_k \leq \sigma$  and  $k < K$ , return the  $\mathbf{x}_k^*$  as optimal solution and terminate the

TABLE I  
DETAILS OF THE EXPERIMENTAL ENVIRONMENT

Term	Configuration
CPU	Intel (R) Core i7-5600@2.60 GHz
RAM	8 GB
Platform	MATLAB 2016
Solver	CPLEX

TABLE II  
THE PARAMETERS OF DERs

	$\bar{P}/P/R$ (kW)	$\alpha$ (\$/kW)	$\beta$ (\$/kW <sup>2</sup> )	$\lambda^{up}/\lambda^{dn}$ (\$/kW)
MT	600/0/240	-	-	1.35/1.35
FC	400/0/130	0.006	0.7	1.05/1.05
EB	250/0/160	-	-	1.00/1.00
PtG	080/0/100	-	-	0.95/0.95

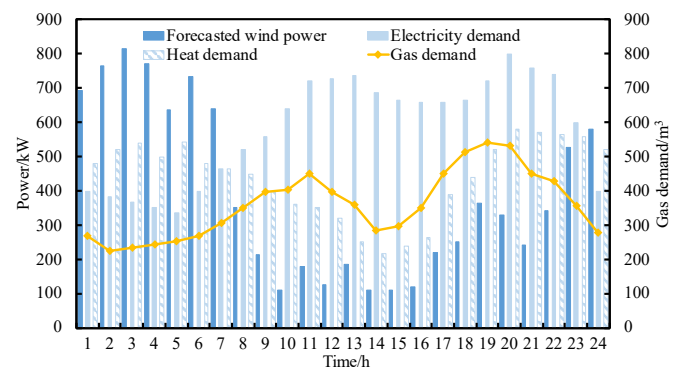


Fig. 3. Load demands and forecasted wind power.

algorithm. Otherwise add new variable  $\mathbf{y}_{k+1}$  and constraint (37), then update  $k = k + 1$  and go to Step 2).

$$\begin{cases} \varphi \geq \mathbf{a}^\top \mathbf{y}_{k+1} + \mathbf{b}^\top \hat{\mathbf{w}}_{k+1} \\ \mathbf{B}\mathbf{x} + \mathbf{D}\mathbf{y}_{k+1} \leq \mathbf{f}, \mathbf{I}\mathbf{y}_{k+1} \leq \hat{\mathbf{w}}_{k+1} \end{cases} \quad (37)$$

#### IV. EXPERIMENTAL RESULTS

The experimental environments are given in Table I. The parameters of FC, MT, EB, and PtG are listed in Table II. The details of ESS and TSS are listed in Table III. The prices of the transaction are given in Table IV. The fluctuations of the electricity, heat, gas demands, and the forecasted WP are shown in Fig. 3. The price of the gas is 0.95\$/m<sup>3</sup>. The cost of the WP curtailment is 0.638\$/kWh. Energy coefficients including  $\eta^{MT}$ ,  $\eta^{PtG}$ ,  $\eta^{EB}$ , and  $\eta^{gas}$  are equal to 0.8, 0.7, 0.9, and 0.8, respectively. The confidence level  $\gamma$  is set to 0.95.

Totally 5 scenarios in Table V are designed to demonstrate the effectiveness of the IEHG-MG operation model. In scenarios #1-#5, TSS, ESS, PtG, and EB are gradually taken into account. Based on scenarios #1-#5, section IV-A investigates the improvements in WP utilization and economics from the deployments of TSS, ESS, PtG, and EB. Moreover, section IV-B compares the presented DRO to the DO, SO, and RO.

To discuss the economics, the following process is designed. First, the two-stage ED model is optimized in the day-

TABLE III  
THE PARAMETERS OF STORAGE SYSTEM

Maximal power (kW)	Initial/Minimal/Maximal SoC (kWh)	$\eta^{dis}/\eta^{cha}$
ESS	300	200/40/0900
TSS	300	200/80/1000

TABLE IV  
TRANSACTION PRICE

	$\lambda^{buy}/\lambda^{sell}$ (\$/kW)	$\rho^{buy}/\rho^{sell}$ (\$/kW)
09:00-12:00 & 19:00-00:00	1.25/1.05	1.55/0.51
08:00-09:00 & 12:00-19:00	0.90/0.78	1.35/0.34
00:00-08:00	0.50/0.35	0.88/0.19

TABLE V  
DETAILS OF SCENARIOS #1-#5

	#1	#2	#3	#4	#5
TSS	✗	✓	✓	✓	✓
ESS	✗	✗	✓	✓	✓
PtG	✗	✗	✗	✓	✓
EB	✗	✗	✗	✗	✓
Optimization method	DO	DO	DO	DO	DO

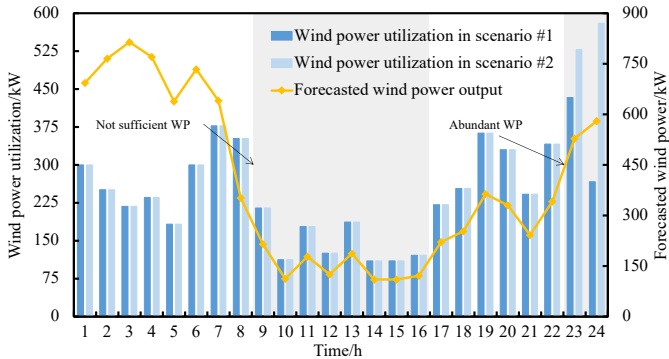


Fig. 4. Utilization of wind power in scenarios #1 and #2.

ahead stage, which delivers *day-ahead dispatch cost*  $C_{DA}$  and *day-ahead operation decision*  $x$ . Then, 500 random WP scenarios are generated following the normal distribution with mean 0 and variance 0.2, which simulates the real-time WP realizations. For each of the 500 random WP scenarios, system conducts real-time adjustments based on decision  $x$ , resulting in an *actual real-time adjustment cost*. Finally, summation of the  $C_{DA}$  and average of the 500 actual real-time adjustment costs serves as the *actual total ED cost* to evaluate the operation economics.

#### A. Improvements of WP Utilization and Economics from Increasing Components

The WP utilizations of scenario #1 and #2 are shown in Fig. 4. The charging power of TSS and output of MT in these two scenarios are shown in Fig. 5.

In scenario #1, the total WP curtailment is 3,598kWh. With the integration of TSS, the WP curtailment falls slightly to

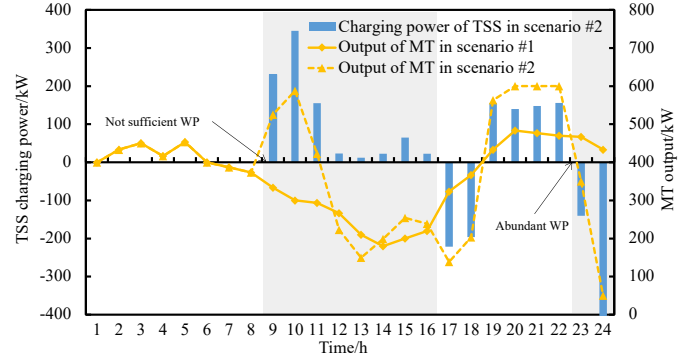


Fig. 5. Outputs of MT and TSS in scenarios #1 and #2.

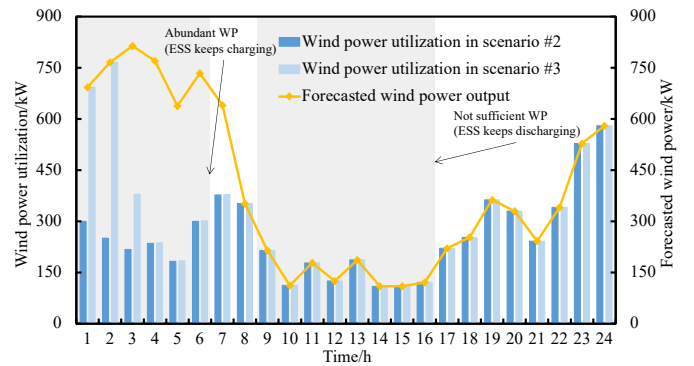


Fig. 6. Utilization of WP in scenarios #2 and #3.

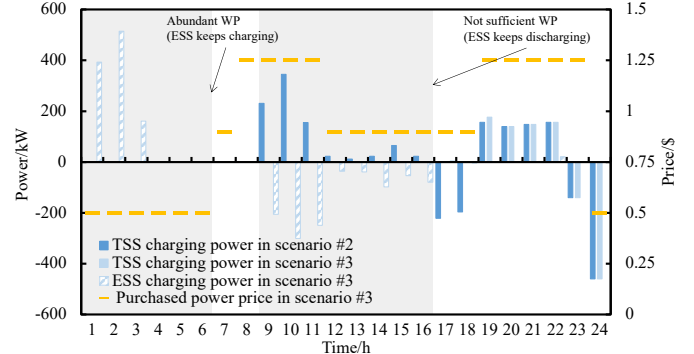


Fig. 7. Outputs of ESS and TSS in scenarios #2 and #3.

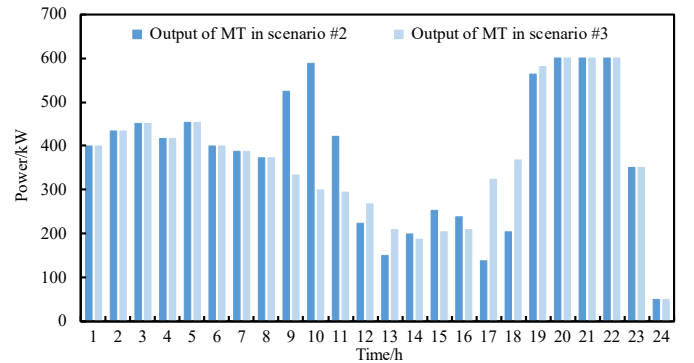


Fig. 8. Output of MT in scenarios #2 and #3.

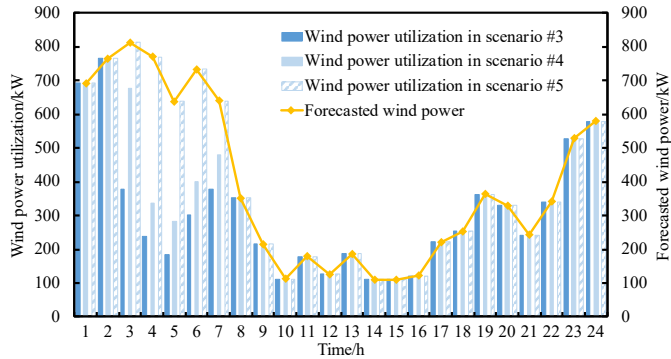


Fig. 9. Utilization of WP in scenarios #3, #4 and #5.

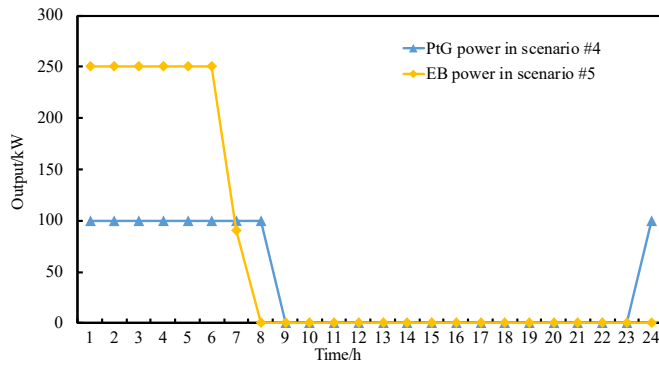


Fig. 10. Outputs of PtG and EB in scenarios #4 and #5.

3,191kWh in scenario #2. As shown in Fig. 4 and Fig. 5, during the 9<sup>th</sup>-16<sup>th</sup> hours, when the WP is not sufficient, the output of MT in scenario #2 is higher than that of scenario #1. TSS absorbs surplus heat power output at the same time. In the 23<sup>rd</sup>-24<sup>th</sup> hour when the WP is abundant, TSS keeps discharging in order to reduce the heat and electricity outputs of MT, creating extra utilization opportunities for surplus WP. To this end, the WP curtailment is successfully reduced with the integration of TSS.

The comparison of the WP utilizations in scenarios #2 and #3 is shown in Fig. 6. The charging and discharging power of ESS and TSS are demonstrated in Fig. 7. The electricity output of MT in these two scenarios is illustrated in Fig. 8.

In scenario #3, the WP curtailment reduces sharply to 2,116 kWh. From Fig. 6 and Fig. 7, it can be observed that ESS keeps charging when the WP is abundant during the 1<sup>st</sup>-6<sup>th</sup> hours, which significantly promotes the utilization for plentiful WP. According to Fig. 7, ESS charges when electricity price is low while discharging when the price is relatively high in the 9<sup>th</sup>-16<sup>th</sup> hours, therefore the cost of purchasing electricity from the grid is reduced. Moreover, compared to scenario #2, TSS is able to charge/discharge less power with the integration of ESS. ESS has also facilitated reducing the heat and electricity outputs of MT by discharging power when the WP is insufficient, as shown in Fig. 6, Fig. 7, and Fig. 8. It is suggested that the coordination of charging and discharging of ESS and TSS is able to decrease the day-ahead dispatch cost and enhance the WP utilization.

We further analyze the effectiveness of PtG and EB. As shown in Fig. 9, the WP curtailment reduces to 1,416kWh in scenario #4, and even no WP curtailment occurs in scenario #5. According to Fig. 9 and Fig. 10, the integration of PtG and EB can significantly promote the utilization of the WP by transforming electricity into natural gas and heat energy respectively, when the WP is sufficient in the 1<sup>st</sup> – 7<sup>th</sup> hours. Additionally, EB can contribute to reducing WP curtailment more significantly than PtG, as the capacity of EB is larger than that of PtG.

TABLE VI  
COMPARISON OF DAY-AHEAD DISPATCH COSTS IN SCENARIOS #1–#5

	#1	#2	#3	#4	#5
Day-ahead dispatch cost (\$)	28,973	27,465	23,853	21,569	<b>17,734</b>

The day-ahead dispatch costs of scenarios #1–#5 are demonstrated in Table VI. As shown in Table VI, the integration of ESS, TSS, PtG, and EB is capable of reducing the day-ahead dispatch cost. From scenarios #1–#5, the WP curtailment is reduced from 3,598kWh to 0kWh, and the day-ahead dispatch cost is decreased from 28,971\$ to 17,734\$. To this end, the results clearly demonstrate that the deployments of TSS, ESS, PtG, and ED significantly improve the flexibility of IEHS-MG, leading to enhanced WP utilization and low day-ahead dispatch cost.

### B. Comparisons of different optimization methods

1) *Data-driven DRO vs DO*: To compare the DRO and the traditional DO, the value of  $\Gamma$  is set to 8, and 10,000 historical data are employed for constructing the ambiguity set.

In Table VII, it can be observed that although the day-ahead dispatch cost of DRO is higher than that of the DO, the average adjustment cost and total actual ED cost of DRO have been considerably reduced compared to those of the DO. This is due to the fact that more resources can be arranged to smooth the uncertainty of WP in the day-ahead ED of the DRO model, which also ensures the economics and robustness as long as the uncertainty is observed.

TABLE VII  
COMPARISON OF OPERATION COSTS BETWEEN DO AND DRO

	DO	DRO
Gas	18,078	18,015
FC	2,399	2,475
Transaction	-2,743	-2,742
Sum	<b>17,734</b>	17,748
Average real-time adjustment cost (\$)	4,508	3,978
Actual total ED cost (\$)	24,042	<b>21,726</b>

2) *Data-driven DRO vs SO*: For the comparison between the presented DRO and SO, the value of  $\Gamma$  is set to 8. Table VIII demonstrates the day-ahead dispatch costs of DRO and SO with the increasing historical data sizes from 10 to 10,000.

TABLE VIII  
COMPARISON OF OPERATION COSTS BETWEEN SO AND DRO

Size of historical data	Optimization method	Day-ahead dispatch cost (\$)	Computation time (s)
10	DRO	17,780	11.3
1,000		17,759	12.1
10,000		17,748	11.1
50	SO	17,744	67.3

As shown in Table VIII, the day-ahead dispatch cost of DRO is higher than that of SO. The day-ahead dispatch cost also decreases gradually as the size of historical data increases. It shows that DRO is more conservative than SO. This is because the objective of the presented DRO is to minimize the day-ahead dispatch cost under the worst-case distribution in the ambiguity set based on the available historical data. However, the actual distribution may differ from the worst-case distribution. By incorporating more historical data, the gap between the day-ahead dispatch costs of SO and DRO reduces gradually. This also reveals the value of the data-driven approach, i.e., the larger size of historical data can shrink the ambiguity set and lead to less-conservative and more-economical dispatch decisions. Moreover, the computational performance is also compared, showing two points: (i) The presented data-driven DRO computationally outperforms SO regardless of the historical data size; and (ii) The computational performance of DRO keeps stable along with the increasing size of historical data.

3) *Data-driven DRO vs RO*: The previous experiments are based on the budget of uncertainty  $\Gamma = 8$ . In this section, three other values  $\Gamma = 0, 16$ , and  $24$  are conducted to study the impact of optimal ED under different uncertainty budgets. RO is also employed for comparison. Here, 10,000 historical data are employed for constructing the uncertainty set of RO and the ambiguity set of DRO. Table IX illustrates the results.

TABLE IX  
COMPARISON OF OPERATION COSTS BETWEEN RO AND DRO

$\Gamma$	Optimization method	Day-ahead dispatch cost (\$)	Average real-time adjustment cost (\$)	Actual total cost (\$)
0	DRO	17734	4508	24042
8		17748	3978	21726
16		17834	3853	21687
24		17859	3853	21712
-	RO	17895	3834	21730

Table IX shows that when  $\Gamma = 0$ , the results of DRO are close to the results of DO. When  $\Gamma$  varies from 8 to 24, the day-ahead dispatch cost of DRO increases. This indicates that if the budget is conservative (i.e., large), more resources are required to smooth the uncertainty of WP but fewer adjustment resources are required once the realization of uncertain WP is revealed. Notably, the day-ahead dispatch cost of DRO is always lower than that of RO. The reason is that RO only focuses on the worst-case observation of the uncertain WP within the given uncertainty set. However, DRO is capable of incorporating partial statistical information to shrink the data-

driven ambiguity set and to obtain less-conservative solutions than RO.

## V. CONCLUSION

To improve the WP utilization and economic operation of an IEHG-MG, this paper presents an IEHG-MG model equipped with ESS, TSS, PtG, and EB. An IDM-based two-stage DRO method is employed to optimize the ED strategy considering WP uncertainty. Finally, C&CG method is employed to solve the model. The experimental results demonstrate the following points.

- The deployments of ESS, TSS, PtG, and EB can significantly improve the flexibility of IEHG-MG. As a result, the WP curtailment can be fully avoided in certain cases, and the operation cost is improved from 28,971\$ to 17,734\$.
- The presented IDM-based DRO is able to effectively handle the WP uncertainty, leading to the lowest operational cost compared to DO and RO.
- Compared to SO, the presented DRO method achieves lower computation time. In addition, the data-driven property of the presented DRO enables its economic performance close to SO, when large-size historical data are available.

In our following-up work, two directions deserve future exploration: (i) The presented system model merely focuses on a general IEHG-MG without complex network constraints. Therefore, it might be valuable to extend the presented system to distribution or transmission scales, in which complex network constraints are incorporated; and (ii) The proposed data-driven DRO method requires operators to tune the budget parameter subjectively. However, it is difficult for an operator to decide which budget value is optimal. Regarding this, [33] discusses a method that can simultaneously optimize dispatch strategies and budget parameters. It should be an interesting direction to investigate the effectiveness of such methods in the presented IEHG-MG.

## REFERENCES

- X. Chen, Y. Yang, Y. Liu *et al.*, “Feature-driven economic improvement for network-constrained unit commitment: A closed-loop predict-and-optimize framework,” *IEEE Trans. Power Syst.*, doi: 10.1109/TPWRS.2021.3128485.
- H. R. Massrur, T. Niknam, M. Fotuhi-Firuzabad, “Investigation of carrier demand response uncertainty on energy flow of renewable-based integrated electricity–gas–heat systems,” *IEEE Trans. Ind. Informat.*, vol. 14, no. 1, pp. 5133–5142, Nov. 2018.
- H. R. Massrur, T. Niknam, J. Aghaei *et al.*, “Fast decomposed energy flow in large-scale integrated electricity–gas–heat energy systems,” *IEEE Trans. Sustain. Energy*, vol. 9, no. 4, pp. 1565–1577, Oct. 2018.
- E. A. M. Ceseña and P. Mancarella, “Energy systems integration in smart districts: robust optimisation of multi-energy flows in integrated electricity, heat and gas networks,” *IEEE Trans. Smart Grid*, vol. 10, no. 1, pp. 1122–1131, Jan. 2019.
- J. Yang, N. Zhang, Y. Cheng *et al.*, “Modeling the operation mechanism of combined P2G and gas-fired plant with CO<sub>2</sub> recycling,” *IEEE Trans. Smart Grid*, vol. 10, no. 1, pp. 1111–1121, Jan. 2019.
- H. Wang, C. Wang, M. Q. Khan *et al.*, “Risk-averse market clearing for coupled electricity, natural gas and district heating system,” *CSEE J. Power Energy Syst.*, vol. 5, no. 2, pp. 240–248, Jun. 2019.
- Y. Li, Y. Zou, Y. Tan *et al.*, “Optimal stochastic operation of integrated low-carbon electric power, natural gas, and heat delivery system,” *IEEE Trans. Sustain. Energy*, vol. 9, no. 1, pp. 273–283, Jan. 2018.

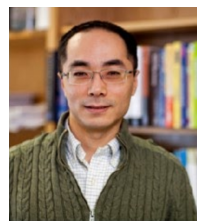
- [8] L. Ni, W. Liu, F. Wen *et al.*, "Optimal operation of electricity, natural gas and heat systems considering integrated demand responses and diversified storage devices," *CSEE J. Power Energy Syst.*, vol. 6, no. 3, pp. 423–437, Jan. 2018.
- [9] Z. Wei, Y. Huang, H. Gao *et al.*, "Joint economic scheduling of power-to-gas and thermoelectric decoupling CHP in regional energy internet," *Power Syst. Tech.*, vol. 42, no. 11, pp. 3512–3519, Nov. 2018.
- [10] Y. Xi, J. Fang, Z. Chen *et al.*, "Optimal coordination of flexible resources in the gas-heat-electricity integrated energy system," *Energy*, vol. 223, pp. 119729, Jan. 2021.
- [11] Z. Li, Y. Xu, S. Fang *et al.*, "Multi-objective coordinated energy dispatch and voyage scheduling for a multi-energy cruising ship," *2019 IEEE/IAS 55th Ind. Com. Power Syst. Tech. Conf. (I&CPS)*, pp. 1–8, Jan. 2019.
- [12] Z. Li and Y. Xu, "Optimal coordinated energy dispatch of a multi-energy microgrid in grid-connected and islanded modes," *Appl. Energy*, vol. 210, pp. 974–986, Jan. 2018.
- [13] J. Wei, Y. Zhang, J. Wang *et al.*, "Distribution LMP-based Demand Management in Industrial Park via a Bi-level Programming Approach," *IEEE Trans. Sustain. Energy*, to be published.
- [14] Z. Li, Y. Xu, S. Fang *et al.*, "Optimal placement of heterogeneous distributed generators in a grid-connected multi-energy microgrid under uncertainties," *IET Renew. Power Gener.*, vol. 13, pp. 2623–2633, Aug. 2019.
- [15] L. Wu, M. Shahidehpour, T. Li, "Stochastic security-constrained unit commitment," *IEEE Trans. Power Syst.*, vol. 22, no. 2, pp. 800–811, May. 2007.
- [16] L. Wu, M. Shahidehpour, Y. Fu, "Security-constrained generation and transmission outage scheduling with uncertainties," *IEEE Trans. Power Syst.*, vol. 25, no. 3, pp. 1674–1685, Aug. 2010.
- [17] L. Wu, M. Shahidehpour, Z. Li, "Comparison of scenario-based and interval optimization approaches to stochastic SCUC," *IEEE Trans. Power Syst.*, vol. 27, no. 2, pp. 913–921, May. 2012.
- [18] C. Dai, L. Wu, H. Wu, "A multi-band uncertainty set based robust SCUC with spatial and temporal budget constraints," *IEEE Trans. Power Syst.*, vol. 31, no. 6, pp. 4988–5000, Nov. 2016.
- [19] B. Hu and L. Wu, "Robust SCUC with multi-band nodal load uncertainty set," *IEEE Trans. Power Syst.*, vol. 31, no. 3, pp. 2491–2492, May. 2016.
- [20] B. Hu and L. Wu, "Robust SCUC considering continuous/discrete uncertainties and quick-start units: a two-stage robust optimization with mixed-integer recourse," *IEEE Trans. Power Syst.*, vol. 31, no. 2, pp. 1407–1419, Mar. 2016.
- [21] Z. Li, Y. Xu, L. Wu *et al.*, "A risk-averse adaptively stochastic method for multi-energy ship operation under diverse uncertainties," *IEEE Trans. Power Syst.*, vol. 36, no. 3, pp. 2149–2161, May. 2021.
- [22] C. He, C. Dai, L. Wu *et al.*, "Robust network hardening strategy for enhancing resilience of integrated electricity and natural gas distribution systems against natural disasters," *IEEE Trans. Power Syst.*, vol. 33, no. 5, pp. 5787–5798, Sept. 2018.
- [23] C. He, L. Wu, T. Liu *et al.*, "Robust co-optimization planning of interdependent electricity and natural gas systems with a joint n-1 and probabilistic reliability criterion," *IEEE Trans. Power Syst.*, vol. 33, no. 2, pp. 2140–2154, Mar. 2018.
- [24] C. He, L. Wu, T. Liu *et al.*, "Robust co-optimization scheduling of electricity and natural gas systems via ADMM," *IEEE Trans. Sustain. Energy*, vol. 8, no. 2, pp. 658–670, Oct. 2016.
- [25] C. He, T. Liu, L. Wu *et al.*, "Robust coordination of interdependent electricity and natural gas systems in day-ahead scheduling for facilitating volatile renewable generations via power-to-gas technology," *CSEE J. Power Energy Syst.*, vol. 5, no. 3, pp. 375–388, Apr. 2017.
- [26] Z. Li, Y. Xu, S. Fang *et al.*, "Robust coordination of a hybrid AC/DC multi-energy ship microgrid with flexible voyage and thermal loads," *IEEE Trans. Smart Grid* doi: 10.1109/TSG.2020.2964831.
- [27] C. He, L. Wu, X. Zhang *et al.*, "Distributionally robust scheduling of integrated gas-electricity systems with demand response," *IEEE Trans. Power Syst.*, vol. 34, no. 5, pp. 3791–3803, Sept. 2019.
- [28] S. He, H. Gao, L. Wang *et al.*, "Distributionally robust planning for integrated energy systems incorporating electric-thermal demand response," *Energy*, vol. 213, pp. 118783, Sept. 2020.
- [29] Y. Zhang, X. Han, M. Yang *et al.*, "Adaptive robust unit commitment considering distributional uncertainty," *Elec. Power Energy Syst.*, vol. 104, pp. 635–644, Jan. 2019.
- [30] L. Wu, "Accelerating NCUC via binary variable-based locally ideal formulation and dynamic global cuts," *IEEE Trans. Power Syst.*, vol. 31, no. 5, pp. 4097–4107, Sept. 2016.
- [31] Y. Xiang, J. Liu, and Y. Liu, "Robust energy management of Microgrid with uncertain renewable generation and load," *IEEE Trans. Smart Grid*, vol. 7, no. 2, pp. 1034–1043, Mar. 2016.
- [32] Z. Li, L. Wu, and Y. Xu, "Risk-averse coordinated operation of a multi-energy microgrid considering voltage/var control and thermal flow: an adaptive stochastic approach," *IEEE Trans. Smart Grid*, vol. 12, no. 5, pp. 3914–3927, Sept. 2021.
- [33] J. Yang and C. Su, "Robust optimization of microgrid based on renewable distributed power generation and load demand uncertainty," *Energy*, vol. 223, no. 15, pp. 120043, May 2021.



**Yang Liu** received the Ph.D. degree from the School of Engineering and Design, Brunel University, London, U.K., in 2011. He is currently an Associate Professor with the College of Electrical Engineering, Sichuan University, Chengdu, China. His research interests include big data analytics, power system planning and dispatching, renewable energy, and integrated energy systems.



**Xianbang Chen** (S'18) received the B.S. and the M.S. degrees in electrical engineering from Sichuan University, Chengdu, China, in 2017 and 2020. Currently, he is pursuing the Ph.D. degree at Stevens Institute of Technology, Hoboken, NJ, USA. His research interests focus on applying data-driven methods on economics operation of power system.



**Lei Wu** (SM'13) received the B.S. degree in electrical engineering and the M.S. degree in systems engineering from Xi'an Jiaotong University, Xi'an, China, in 2001 and 2004, respectively, and the Ph.D. degree in electrical engineering from Illinois Institute of Technology (IIT), Chicago, IL, USA, in 2008. From 2008 to 2010, he was a Senior Research Associate with the Robert W. Galvin Center for Electricity Innovation, IIT. He was a summer Visiting Faculty at NYISO in 2012. He was a Professor with the Electrical and Computer Engineering Department, Clarkson University, Potsdam, NY, USA, till 2018. He is currently a Professor with the Electrical and Computer Engineering Department, Stevens Institute of Technology, Hoboken, NJ, USA. His research interests include power systems operation and planning, energy economics, and community resilience microgrid.



**Yanli Ye** received the B.S. and the M.S. degrees in electrical engineering from Sichuan University, Chengdu, China, in 2017 and 2020. Her research interests focus on applying optimization methods on microgrid operation.